miR-155 modulates high glucose-induced cardiac fibrosis via the Nrf2/HO-1 signaling pathway

YU LI[1], JING-ZHU DUAN[2], QIAN HE[1] and CHONG-QUAN WANG[1]

Departments of [1]Cardiology and [2]Respiratory Medicine, Taihe Hospital, Hubei University of Medicine, Shiyan, Hubei 442000, P.R. China

Received May 8, 2019; Accepted January 29, 2020

DOI: 10.3892/mmr.2020.11495

Abstract. Cardiac fibrosis is a major pathological manifestation of diabetic cardiomyopathy, which is a leading cause of mortality in patients with diabetes. MicroRNA (miR)-155 is upregulated in cardiomyocytes in cardiac fibrosis, and the aim of the present study was to investigate if the inhibition of miR-155 was able to ameliorate cardiac fibrosis by targeting the nuclear factor erythroid-2-related factor 2 (Nrf2)/heme oxygenase-1 (HO-1) signaling pathway. H9C2 rat cardiomyocytes were cultured with high glucose (HG; 30 mM) to establish an *in vitro* cardiac fibrosis model that mimicked diabetic conditions; a miR-155 inhibitor and a miR-155 mimic were transfected into H9C2 cells. Following HG treatment, H9C2 cells exhibited increased expression levels of miR-155 and the fibrosis markers collagen I and α-smooth muscle actin (α-SMA). In addition, the expression levels of endonuclear Nrf2 and HO-1 were decreased, but the expression level of cytoplasmic Nrf2 was increased. Moreover, oxidative stress, mitochondrial damage and cell apoptosis were significantly increased, as indicated by elevated reactive oxygen species, malonaldehyde and monomeric JC-1 expression levels. In addition, superoxide dismutase expression was attenuated and there was an increased expression level of released cytochrome-*c* following HG treatment. Furthermore, it was demonstrated that expression levels of Bcl-2 and uncleaved Poly (ADP-ribose) polymerase were downregulated, whereas Bax, cleaved caspase-3 and caspase-9 were upregulated after HG treatment. However, the miR-155 inhibitor significantly restored Nrf2 and HO-1 expression levels, and reduced oxidative stress levels, the extent of mitochondrial damage and the number of cells undergoing apoptosis. Additionally, the miR-155 inhibitor significantly reversed the expression levels of collagen I and α-SMA, thus ameliorating fibrosis. Furthermore, the knockdown of Nrf2 reversed the above effects induced by the miR-155 inhibitor. In conclusion, the miR-155 inhibitor may ameliorate diabetic cardiac fibrosis by reducing the accumulation of oxidative stress-related molecules, and preventing mitochondrial damage and cardiomyocyte apoptosis by enhancing the Nrf2/HO-1 signaling pathway. This mechanism may facilitate the development of novel targets to prevent cardiac fibrosis in patients with diabetes.

Correspondence to: Dr Chong-Quan Wang, Department of Cardiology, Taihe Hospital, Hubei University of Medicine, 32 South Renmin Road, Shiyan, Hubei 442000, P.R. China
E-mail: wangchongquan13@163.com

Key words: microRNA-155, nuclear factor erythroid-2-related factor 2/heme oxygenase-1 signaling pathway, oxidative stress, mitochondrial injury, apoptosis, cardiac fibrosis

Introduction

Cardiac fibrosis is a worldwide health issue associated with nearly all forms of heart disease, such as ventricular dilation and heart failure (1), which accounts for nearly 31% of all deaths each year (2). Fibrosis pathogenesis mainly involves inappropriate fibroblast accumulation and excess collagen deposition in the myocardium (3), which is accompanied by excessive oxidative stress and apoptosis or necrosis of cardiomyocytes (4). Acute myocardial infarction, ageing, pressure overload, volume overload, hypertrophic cardiomyopathy and post-viral dilated cardiomyopathy are common pathophysiological conditions that induce cardiac fibrosis (5). Moreover, metabolic disorders such as diabetes and obesity are involved in the formation of fibrosis in the myocardium of patients (6,7). A previous study reported that cardiac fibrosis is closely associated with the progression of diabetic cardiomyopathy, which is a major cause of mortality in patients with diabetes (8). Thus, it is crucial to develop novel targets to suppress apoptosis of cardiomyocytes, and to prevent the formation of diabetic cardiac fibrosis and cardiomyopathy.

MicroRNAs (miRNAs) are small non-coding RNAs that are involved in the regulation of gene expression at the post-transcriptional level (9). It has been demonstrated that miRNAs serve a significant role in cardiovascular diseases (10); for example, miR-155 dysregulation is essential for cardiac pathophysiology, including hypertrophy, remodeling and fibrosis. Loss of miR-155 can inhibit pathological cardiac hypertrophy (11), whereas cardiac fibrosis is usually associated with elevated miR-155 expression levels (12). However, the downstream signaling pathways of miR-155 that regulate myocardial fibrosis have not been fully elucidated.

Nuclear factor erythroid-2-related factor 2 (Nrf2) is a transcription factor with a basic-leucine zipper domain that can

regulate various antioxidant proteins (13). The Nrf2 signaling pathway is implicated in the amelioration of cardiac fibrosis by regulating oxidative stress and cell apoptosis (14,15). Heme oxygenase-1 (HO-1) is an antioxidative gene, and its expression is initiated and promoted by Nrf2 (16). The HO-1 protein degrades heme into biliverdin, ferrous iron and carbon monoxide, and thus is able to ameliorate cellular injury by exerting antioxidant effects (17). Nrf2/HO-1 signaling was demonstrated to be increased in an overpressure-induced cardiac fibrosis model (15) and in a doxorubicin-induced oxidative injury model (18), and this enhanced anti-oxidative effect is essential for inhibiting fibrosis and injury. Although previous studies have found that miR-155 modulates oxidative stress by targeting the Nrf2-mediated signaling pathway in various diseases (19-21), the specific association between miR-155 and the Nrf2/HO-1 signaling pathway in the progression of cardiac fibrosis remains largely unknown.

The present study established a high glucose (HG)-induced cardiac fibrosis cell model by culturing H9C2 cells with 30 mM glucose, which mimics the diabetes-induced cardiomyopathy condition (22). It has been reported that HG treatment can increase the activity of the transcriptional co-regulator p300 and also enhance transforming growth factor-β (TGF-β) signaling through SMAD2 acetylation (23), which then promotes the formation of cardiac fibrotic tissue (11). Results from the present study suggested that miR-155 impaired the Nrf2/HO-1 signaling pathway to induce oxidative stress, promote mitochondrial injury and cardiomyocyte apoptosis, and increase extracellular matrix accumulation in the cardiac fibrosis model. To the best of our knowledge, the present study is the first to indicate that miR-155 targeting the Nrf2/HO-1 signaling pathway may regulate cardiac fibrosis. Moreover, this mechanism may be a potential therapeutic target for cardiac fibrosis treatment.

Materials and methods

Cell culture. H9C2 rat cardiomyocytes (American Type Culture Collection) were cultured in DMEM (Gibco; Thermo Fisher Scientific, Inc.) supplemented with 10% FBS (Gibco; Thermo Fisher Scientific, Inc.) and 1% penicillin and streptomycin (Gibco; Thermo Fisher Scientific, Inc.), and were maintained at 37˚C in a humidified incubator with 5% CO_2. To induce HG-mediated fibrosis, the H9C2 cells were cultured with 30 mM glucose (Sigma-Aldrich; Merck KGaA) at 37˚C for 24 or 48 h.

Cell transfection. H9C2 cells ($2x10^5$) were seeded in 6-well plates and cultured at 37˚C for 24 h. Before transfection, the DMEM was replaced with serum-free DMEM medium (Gibco; Thermo Fisher Scientific, Inc.) for a further 24 h of culturing at 37˚. Then, miR-155 inhibitor (5'-ACCCCUAUCACGAUUAGCAUUAA-3') or miR-155 mimics (sense 5'-UUAAUGCUAAUCGUGAUAGGGGUU-3', antisense 5'-CCCCUAUCACGAUUAGCAUUAAUU-3') miRNAs (10 nM, Invitrogen; Thermo Fisher Scientific, Inc.) were transfected for 6 h into H9C2 cells at 37˚C using Lipofectamine® RNAi MAX transfection reagent (Invitrogen; Thermo Fisher Scientific, Inc.), followed by exposure to normal glucose (NG; 5 mM) or HG (30 mM) treatment for 24 or 48 h at 37˚C. The cells were subsequently collected for western blot analysis, reverse transcription-quantitative PCR (RT-qPCR), mitochondrial membrane potential measurement, and oxidative stress and cell apoptosis assays.

Plasmid construction for short hairpin RNA (shRNA)-mediated knockdown. H9C2 cells ($2x10^5$) were seeded in 6-well plates and cultured at 37˚C for 24 h. A pGPH1 plasmid expressing shRNA targeting Nrf2 (shNrf2, 5'-CCGGAGTTTGGGAGG AGCTATTATCCTCGAGGATAATAGCTCCTCCCAAAC TTTTTTG-3') and a scrambled control shRNA-expressing pGPH1 plasmid (shNC, 5'-CCGGCCTAAGGTTAAGTC GCCCTCGCTCGAGCGAGGGCGACTTAACCTTAGGTT TTTG-3') were purchased from Shanghai GenePharma Co., Ltd. Lipofectamine 2000 (3 µl/well; Thermo Fisher Scientific, Inc.) and 1 µg/well pGPH1 plasmids were mixed and added to cells according to the manufacturer's instructions. Then the cells were cultured for another 48 h at 37˚C before subsequent experiments.

Apoptosis analysis with Annexin V/PI staining. Cell apoptosis was measured using an Annexin V-FITC/PI dual staining kit (Thermo Fisher Scientific, Inc.) according to the manufacturer's instructions. H9C2 cells were trypsinized, collected and washed once with cold PBS. After centrifugation at 4˚C, 200 x g for 5 min, the cells were collected and concentrated to $1x10^5$ cells per ml. A 0.1 ml sample solution was mixed with 5 µl of Annexin V-FITC and 5 µl of propidium iodide (PI) solution, and incubated for 15 min at room temperature. After mixing, the cell samples were subjected to flow cytometry (FACSCalibur; BD Biosciences) analysis. A total of 10,000 cells were analyzed by flow cytometry. The apoptotic cell rate was analyzed via FlowJo software (version 10; FlowJo LLC) and calculated by adding the proportions of early apoptotic cells (Annexin V-FITC$^+$PI$^-$) and late apoptotic cells (Annexin V-FITC$^+$PI$^+$).

Reactive oxygen species (ROS) analysis. The level of intracellular ROS was determined using a dichloro-dihydro-fluorescein diacetate (DCFH-DA) assay (Nanjing Jiancheng Bioengineering Institute) and a ROS assay kit (Nanjing Jiancheng Bioengineering Institute). First, H9C2 cells were cultured with 10 µM DCFH-DA at 37˚C for 30 min, and then harvested by trypsinization and washed once with PBS. Next, the cells were resuspended in PBS and the cell density was adjusted to $1x10^6$ cells/ml. The fluorescence intensity of the DCF was measured with a Synergy MX Multi-Mode microplate reader (BioTek Instruments, Inc.) with the excitation wavelength at 480 nm and the emission wavelength at 525 nm, which were used to determine the intracellular ROS levels.

Superoxide dismutase (SOD) and malonaldehyde (MDA) measurements. The activities of MDA and SOD in H9C2 cells were also assessed using Malondialdehyde (MDA) and Superoxide Dismutase (SOD) assay kit (Nanjing Jiancheng Bioengineering Institute). H9C2 cells were collected using a rubber scraper and homogenized in cold buffer (10 mM Tris-HCl; 0.25 M sucrose; and 25 mM phenylmethylsulfonyl fluoride, pH 7.4). A total of 0.1 ml homogenate was mixed with 1 ml MDA working solution and incubated at 95˚C for 40 min.

Table I. Primers sequences used for reverse transcription-quantitative PCR.

Gene	Primer sequence (5'→3')
GAPDH	F: CGCTAACATCAAATGGGGTG
	R: TTGCTGACAATCTTGAGGGAG
U6	F: CTCGCTTCGGCAGCACA
	R: AACGCTTCACGAATTTGCGT
MicroRNA-155	F: TGCCTCCAACTGACTCCTAC
	R: GCCAGCAGAATAATACGAC
α-smooth muscle actin	F: AGCATCCGACCTTGCTAACG
	R: TGAGTCACGCCATCTCCAGAG
Collagen I	F: TTTAATGGATAGGGACTTGTGTGAA
	R:GAGAGAGAGAGAAGCTGAGGGTAGG

F, forward; R, reverse.

The samples were cooled and centrifuged at 200 x g, 22˚C for 10 min, and then 250 μl of supernatant was loaded into 96-well plate. The optical density (OD) of each well was measured at 530 nm wavelength (OD530) with a microplate reader. For the SOD assay, 0.1 ml of the homogenate was sequentially mixed with 20 μl enzyme working liquid and 200 μl substrate reaction solution, according to the manufacturer's instructions, and then incubated at 37˚C for 40 min. SOD activity was then assessed by measuring the OD550 with a spectrophotometer. The values of MDA and SOD were used as indicators of lipid superoxide and oxygen free radical in the cardiomyocytes, respectively.

Mitochondrial membrane potential measurement by JC-1 assay. The mitochondrial membrane potential was measured using a JC-1 Mitochondrial Membrane Potential assay kit (Cayman Chemical Company). H9C2 cells were seeded ($1x10^5$ cells/well) in a 24-well plate in DMEM with NG or HG for 24 or 48 h. Next, JC-1 staining solution (100 μl/ml of medium/well) was loaded into each well of the plate and mixed for 10 sec at 25˚C, and the cells were cultured in a CO_2 incubator at 37˚C for 15 min. Subsequently, the plate was centrifuged at 400 x g at 25˚C for 5 min and the supernatant was discarded. The plate was washed twice with 500 μl of assay buffer (supplied as part of the JC-1 kit), and then the cells were covered with 250 μl of assay buffer. The cells were then analyzed with a TS100 fluorescence microscope (magnification, x200; Nikon Corporation). Normal cells (cells that did not receive treatment) with aggregated JC-1 were captured with the fluorescence microscopy filter set for red fluorescent dye (excitation/emission=540/570 nm), and apoptotic cells with monomeric JC-1 were detected with the fluorescence microscopy filter set for green fluorescent dye (excitation/emission =485/535 nm).

RT-qPCR. TRIzol reagent (Invitrogen; Thermo Fisher Scientific, Inc.) was used to extract the total RNA from H9C2 cells. After quantification using a NanoDrop ND-1000 spectrophotometer (NanoDrop Technologies; Thermo Fisher Scientific), 2 μg total RNA was applied to generate the first-strand cDNA at 25˚C for 5 min, 37˚C for 30 min and 85˚C for 5 sec with First Strand cDNA Synthesis kit (Sigma-Aldrich; Merck KGaA) according to the manufacturer's instructions. qPCR experiments were performed on an ABI 7300 thermocycler (Applied Biosystems; Thermo Fisher Scientific, Inc.) with SYBR-Green dye (Invitrogen; Thermo Fisher Scientific, Inc.). The thermocycling conditions were as follows: Initial denaturation, 95˚C for 5 sec; followed by 35 cycles of denaturation at 94˚C for 15 sec, annealing at 55˚C for 25 sec and extension at 70˚C for 30 sec. GAPDH was used as the internal reference for mRNA, and U6 small nuclear RNA (U6 snRNA) was used as the miRNA control. The relative expression of a target gene was calculated with the $2^{-\Delta\Delta Cq}$ method (24). The specific primers used for qPCR are listed in Table I.

Endonuclear, cytoplasmic and mitochondrial protein extraction. Endonuclear proteins and cytoplasmic proteins were obtained using Cell Nuclear and Cytoplasmic Protein Extraction kit (Beyotime Institute of Biotechnology), according to the manufacturer's protocol. After being washed with PBS, $1x10^7$ H9C2 cells were detached from the dish using a rubber scraper, and then collected and centrifuged at 4˚C, 200 x g for 5 min. After the supernatant was aspirated, the cell pellet was resuspended with cytoplasmic protein extraction reagent A [supplemented with 1 mM PMSF (Sigma-Aldrich; Merck KGaA)], vortexed for 5 sec and incubated on ice for 15 min. Then, the cell samples were mixed with cytoplasmic protein extraction reagent B, vortexed for 5 sec and incubated on ice for 1 min. Cells were vortexed again for 5 sec, centrifuged at 4˚C at 16,000 x g for 5 min and the supernatant, which contained the cytoplasmic proteins, was collected and transferred to a new tube. The remaining pellet in the tube was then re-suspended with nuclear protein extraction reagent (supplemented with 1 mM PMSF) and further homogenized by cycles of vigorous vortex mixing for 15-30 sec followed by incubation on ice for 1-2 min for 30 min. After centrifugation at 16,000 x g at 4˚C for 10 min, the supernatant containing the nuclear proteins was transferred to a cold tube.

Mitochondrial and cytoplasmic proteins were obtained with a Cell Mitochondria Isolation kit (cat. no. C3601; Beyotime Institute of Biotechnology), following the manufacturer's protocol. H9C2 cells were trypsinized, washed once

with cold PBS and resuspended in mitochondria isolation buffer (supplied as part of the Cell Mitochondria Isolation kit) supplemented with 1 mM PMSF and incubated on ice for 15 min. Next, the samples were homogenized and centrifuged at 4˚C at 600 x g for 15 min. The supernatant was collected and transferred to a clean tube, which was then centrifuged at 4˚C at 11,000 x g for 15 min. The supernatant, which contained the cytoplasmic proteins, was collected in a new 1.5 ml eppendorf tube and the pellet, which contained the isolated mitochondria, was subjected to mitochondria lysis buffer supplemented with 1 mM PMSF. Following the lysis of mitochondria, all the mitochondrial proteins were released in the lysis buffer. The endonuclear, cytoplasmic and mitochondrial proteins were then analyzed by western blotting, as described in the following method.

Western blot analysis. A total of $1x10^7$ cells were harvested and lysed in RIPA cell lysis buffer (150 mM NaCl; 50 mM Tris-HCl; 0.5% sodium deoxycholate; 1% NP-4; 0.1% SDS, pH 7.4; and 1X protease inhibitor cocktail; Selleck Chemicals] and rotated for 1 h at 4˚C. Next, the cell lysates were centrifuged at 4˚C at 1,200 x g for 10 min, and the supernatant was collected. Protein concentrations were determined with a commercial bicinchoninic acid protein assay kit (Tiangen Biotech Co., Ltd.). 30 μg protein samples were subjected to 10% SDS-PAGE and transferred onto PVDF membranes (EMD Millipore). After blocking with 5% skim milk (EMD Millipore) for 1 h at 25˚C, the PVDF membranes were probed with primary antibodies against α-SMA (1:1,000; cat. no. ab5694; Abcam), collagen I (1:2,000; cat. no. ab34710; Abcam), Nrf2 (1:1,000; cat. no. ab62352; Abcam), HO-1 (1:1,000; cat. no. ab 13248; Abcam), cytochrome-*c* (Cyt-*c*; 1:1,000; cat. no. ab13575; Abcam), cytochrome-*c* oxidase subunit IV (COX IV; 1:1,000; cat. no. ab33985; Abcam), Lamin B1 (1:5,000; cat. no. ab16048; Abcam), cleaved Caspase-3 (1:2,000; cat. no. 9661; Cell Signaling Technology, Inc.), cleaved Caspase-9 (1:1,000; cat. no. 7237; Cell Signaling Technology, Inc.), poly (ADP-ribose) polymerase (PARP; 1:2,000; cat. no. 9532; Cell Signaling Technology, Inc.), Bax (1:2,000; cat. no. 5023; Cell Signaling Technology, Inc.), Bcl-2 (1:2,000; cat. no. 12789-1-AP; ProteinTech Group, Inc.) and GAPDH (1:5,000; cat. no. 60004-1-Ig ProteinTech Group, Inc.) at 4˚C overnight. After washing three times with TBST (20 mM Tris, 137 mM NaCl, 0.1% Tween-20), the membranes were then probed with horseradish peroxidase-conjugated goat anti-mouse or anti-rabbit (both 1:5,000; cat. nos. 7076 and 7074, respectively; both Cell Signaling Technology, Inc.) antibody for 1 h at room temperature. Protein bands were visualized using an ECL reagent (EMD Millipore), captured using a LAS-3000 imager (Fuji Film Corporation) and semi-quantified using ImageJ software (version 1.52, National Institutes of Health). The protein expression levels were normalized to the controls.

Statistical analysis. Each experiment was performed at least times, and representative data from one replicate are shown in the figures. Data are presented as the mean ± SD. Statistical analysis was performed using a one-way ANOVA followed by Tukey's post hoc test, using SPSS software version 13.0 (SPSS, Inc.). $P<0.05$ was considered to indicate a statistically significant difference.

Results

Effects of miR-155 in the HG-induced cardiac fibrosis model. H9C2 cells were treated with a high concentration of glucose (30 mM) for 24 h to establish a cardiac fibrosis model at the cellular level. The expression level of miR-155 was assessed using RT-qPCR, which demonstrated that HG treatment resulted in increased miR-155 expression compared with NG-treated cells (Fig. 1A). In addition, the effects of miR-155 inhibitors and miR-155 mimics in both NG- and HG-treated H9C2 cells were examined. It was shown that the miR-155 inhibitor suppressed miR-155 expression levels, whereas the miR-155 mimics significantly increased miR-155 expression levels, regardless of NG or HG treatment (Fig. 1A). The expression levels of collagen I and α-SMA in NG- and HG-treated H9C2 cells, both of which were positively associated with fibrosis, were also examined. Western blot analysis results indicated that both collagen I and α-SMA protein expression levels were significantly increased after HG treatment (Fig. 1B). In addition, inhibiting miR-155 expression led to significantly reduced collagen I and α-SMA expression levels, whereas overexpression of miR-155 increased the expression levels. Moreover, the mRNA expression levels of α-SMA and collagen I were also downregulated when miR-155 expression levels were impaired, although there were no significant differences in collagen I expression levels in the NG and HG groups, and α-SMA expression levels in the NG group. However, miR-155 overexpression upregulated α-SMA and collagen I mRNA expression levels in both the NG and HG groups (Fig. 1C). Therefore, these results suggested that the cardiac fibrosis model was successfully established.

In addition, apoptotic rates were examined by flow cytometry. It was demonstrated that the miR-155 mimics further increased the number of apoptotic cells, whereas the miR-155 inhibitor suppressed apoptosis compared with the Control (Fig. 1D). Collectively, the results suggested that miR-155 was upregulated in the HG-induced cardiac fibrosis cell model, which indicated that miR-155 may be involved in cardiac fibrosis, extracellular matrix deposition and cardiomyocyte apoptosis. In addition, it was shown that the miR-155 mimics contributed to the fibrotic phenotypes, whereas the miR-155 inhibitor prevented the acquisition of the fibrotic phenotypes.

miR-155 inhibition partially restores the Nrf2/HO-1 signaling pathway induced by HG. The role of the miR-155 inhibitor on the Nrf2/HO-1 signaling pathway in the HG-induced cardiac fibrosis model was investigated. It was demonstrated that HG treatment for 48 h increased the expression levels of miR-155 in H9C2 cells compared with the levels produced after 24 h of treatment. miR-155 inhibitor transfection significantly reduced miR-155 expression levels that had been induced by HG at both 24 and 48 h (Fig. 2A). The effects of the miR-155 inhibitor on the expression levels of Nrf2 and HO-1 in HG-treated H9C2 cells were also examined. Western blot analysis results indicated that HG treatment downregulated endonuclear Nrf2 expression level and upregulated cytoplasmic Nrf2 expression level compared with the control group (Fig. 2B and C). As a downstream antioxidative protein induced after endonuclear Nrf2-mediated transcriptional activation (16), HO-1 was identified to have similar expression levels as endonuclear

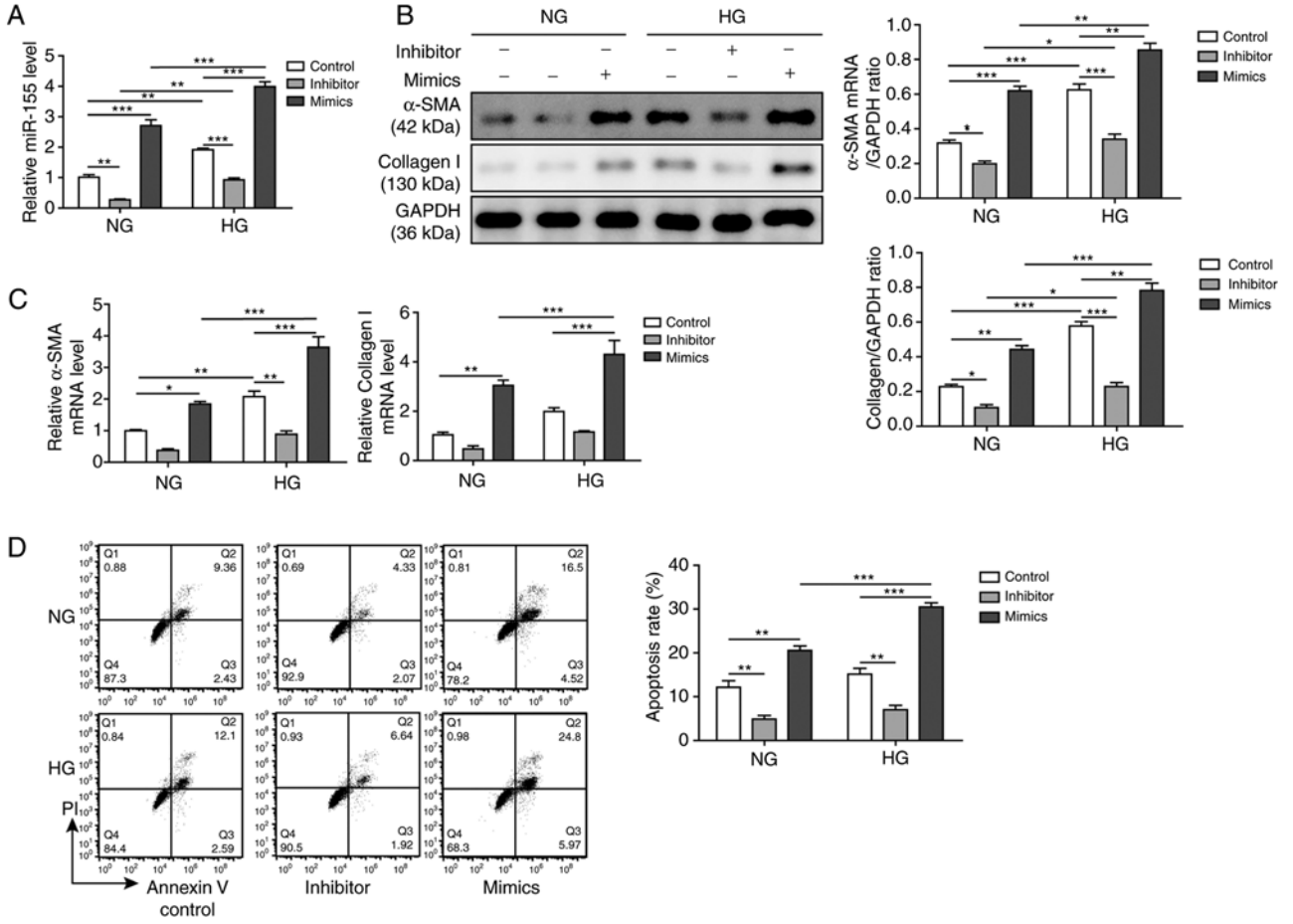

Figure 1. Effects of miR-155 on cardiac fibrosis induced by HG *in vitro*. H9C2 cells transfected with a miR-155 inhibitor or a miR-155 mimic were co-treated with NG (5 mM) or HG (30 mM) for 24 h. (A) Relative mRNA expression levels of miR-155 were measured by RT-qPCR. (B) Protein expression levels of α-SMA and collagen I were assessed by western blotting and semi-quantitated; GAPDH was used as the loading control and for normalization. (C) Relative mRNA expression levels of α-SMA and collagen I. (D) Apoptotic rates were determined by Annexin V-FITC/PI staining and flow cytometry. Data are presented as the mean ± SD from three independent experiments. *P<0.05, **P<0.01 and ***P<0.001. α-SMA, α-smooth muscle actin; HG, high glucose; miR-155, microRNA-155; NG, normal glucose; PI, propidium iodide; RT-qPCR, reverse transcription-quantitative PCR.

Nrf2. However, the miR-155 inhibitor reversed these changes, most notably in HG-cells treated for 48 h (Fig. 2B and C). It was demonstrated that miR-155 inhibition enhanced nuclear translocation of Nrf2 and increased the expression level of HO-1 in HG-treated H9C2 cells (Fig. 2C). Collectively, the present results indicated that miR-155 may modulate HG-induced cardiac fibrosis by targeting the Nrf2/HO-1 signaling pathway.

Inhibiting miR-155 reduces oxidative stress and mitochondrial damage induced by HG. Since oxidative stress and mitochondrial injury are the main manifestations of cardiac fibrosis (25), and as miR-155 regulates oxidative stress by targeting the Nrf2-mediated signaling pathway in some diseases (16-18), the present study examined miR-155 regulation of oxidative stress and mitochondrial injury in HG-treated H9C2 cells. It was demonstrated that HG treatment significantly increased ROS and MDA expression levels, and decreased SOD expression levels in H9C2 cells compared with control cells at both 24 and 48 h (Fig. 3A-C, respectively), which indicated that substantial oxidative stress occurred. However, miR-155 inhibition reversed the increased ROS and MDA levels and the decreased SOD levels, suggesting that an antioxidative response may be triggered and enhanced by miR-155 attenuation (Fig. 3A-C). Cyt-*c* is an important component of the electron transport chain, and is localized in the spaces between the intermembrane and the cristae of mitochondria (26). Generally, ROS production in mitochondria results in the release of Cyt-*c* from the mitochondria into the cytosol and initiates cell apoptosis (27). Therefore, the present study assessed the content of mitochondrial and cytoplasmic Cyt-*c* in HG-treated H9C2 cells to investigate the effect of miR-155 on mitochondrial damage. The western blot analysis results indicated that HG treatment induced the release of Cyt-*c* from the mitochondria into the cytosol, particularly in the H9C2 cells that were treated for 48 h (Fig. 3D and E). However, miR-155 inhibition partially prevented the release of Cyt-*c* into the cytosol, as determined by increased protein expression levels of mitochondrial Cyt-*c* and decreased levels of cytoplasmic Cyt-*c* (Fig. 3D and E).

In addition, mitochondria membrane potential was examined using a JC-1 assay. It was found that HG treatment impaired the integrity of mitochondria in H9C2 cells, which led to a reduced membrane potential as indicated by elevated

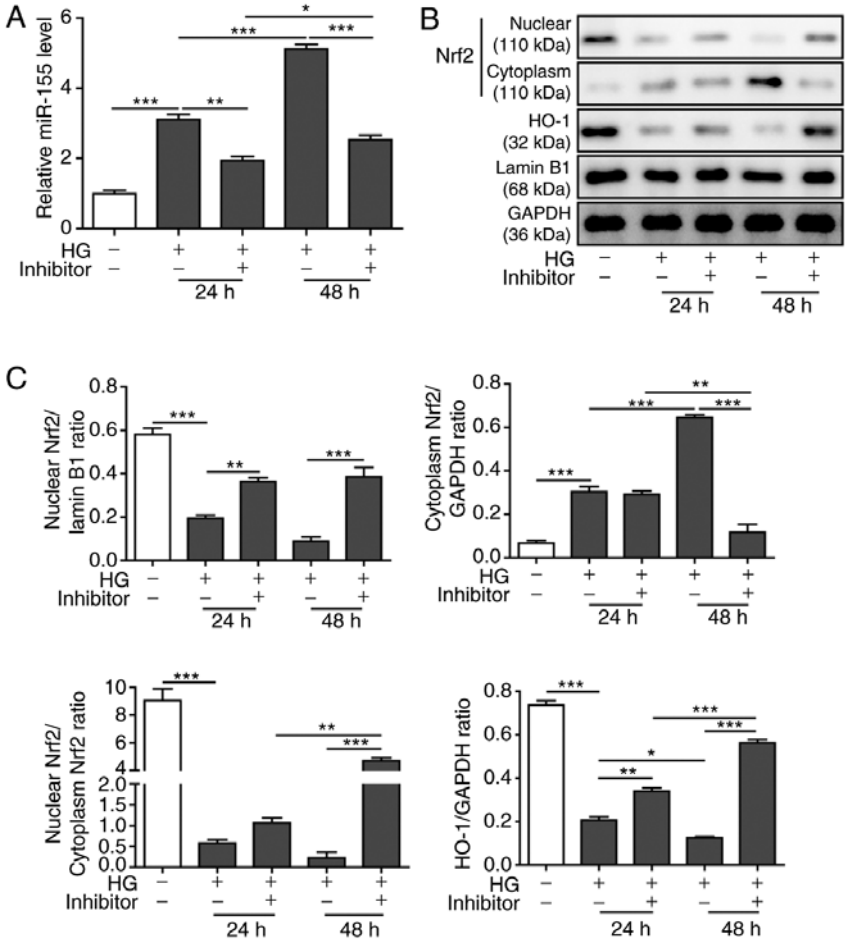

Figure 2. Effects of miR-155 inhibitor on the HG-induced Nrf2/HO-1 signaling pathway. H9C2 cells were treated with HG and co-transfected with or without miR-155 inhibitor for 24 and 48 h. (A) Relative mRNA expression levels of miR-155 were measured by reverse transcription-quantitative PCR. (B) Protein expression levels of endonuclear and cytoplasmic Nrf2, and HO-1 in whole cell lysate were assessed by western blot analysis; Lamin B1 and GAPDH were used as the nuclear and cytoplasmic fraction loading controls, respectively. (C) Semi-quantification of endonuclear and cytoplasmic Nrf2 expression levels and HO-1 protein expression levels after normalization to Lamin B1 and GAPDH. The ratio of normalized endonuclear Nrf2 to cytoplasmic Nrf2 is also shown. Data presented as the mean ± SD from three independent experiments. *P<0.05, **P<0.01 and ***P<0.001. HG, high glucose; HO-1, heme oxygenase-1; miR-155, microRNA-155; Nrf2, nuclear factor erythroid-2-related factor 2.

JC-1 monomer and decreased JC-1 aggregation (Fig. 3F). In addition, miR-155 inhibitor transfection significantly repressed the downregulation of the membrane potential of the mitochondria in H9C2 cells after HG treatment, which suggested that miR-155 inhibition may aid in relieving mitochondrial damage under HG conditions. Overall, these results indicated that inhibition of miR-155 suppressed oxidative stress and mitochondrial damage in the HG-induced cardiac fibrosis model.

miR-155 inhibition suppresses the apoptosis of cardiomyocytes induced by HG. Excessive oxidative stress and mitochondrial damage lead to cell apoptosis, which is one of the causes of cardiac fibrosis (28). To investigate the function of miR-155 on the apoptosis of cardiomyocytes, western blotting was performed to assess the protein expression levels of apoptosis-associated proteins in HG-treated H9C2 cells. The present results suggested that the protein expression levels of Bcl-2, an anti-apoptotic protein (29), were downregulated, and Bax, a pro-apoptotic protein (30), were upregulated after HG treatment (Fig. 4A). Moreover, the protein expression levels of the activated caspases, cleaved caspase-3 and caspase-9, were increased, and the uncleaved PARP expression levels were decreased (Fig. 4A). This phenotype indicated that HG-induced cardiomyocyte apoptosis may be mediated by the caspase-9-dependent mitochondrial damage pathway. In addition, the decreased expression levels of anti-apoptotic proteins and the enhanced expression levels of pro-apoptotic proteins had a time-dependent effect (Fig. 4A). However, miR-155 inhibition reversed the expression levels of the apoptosis-associated proteins in H9C2 cells (Fig. 4A). In addition, it was demonstrated that HG treatment increased the number of apoptotic cells compared with the control treated cells, and this result had a time-dependent trend (Fig. 4B). Additionally, miR-155 inhibition reduced the total apoptotic rate. Taken together, these results suggested that miR-155 inhibition suppressed HG-induced apoptosis in cardiomyocytes.

miR-155 inhibition mitigates cardiac fibrosis induced by HG. The progression of cardiac fibrosis is characterized by the abnormal expression and secretion of collagen I and α-SMA in cardiomyocytes (31). To investigate the effect of miR-155

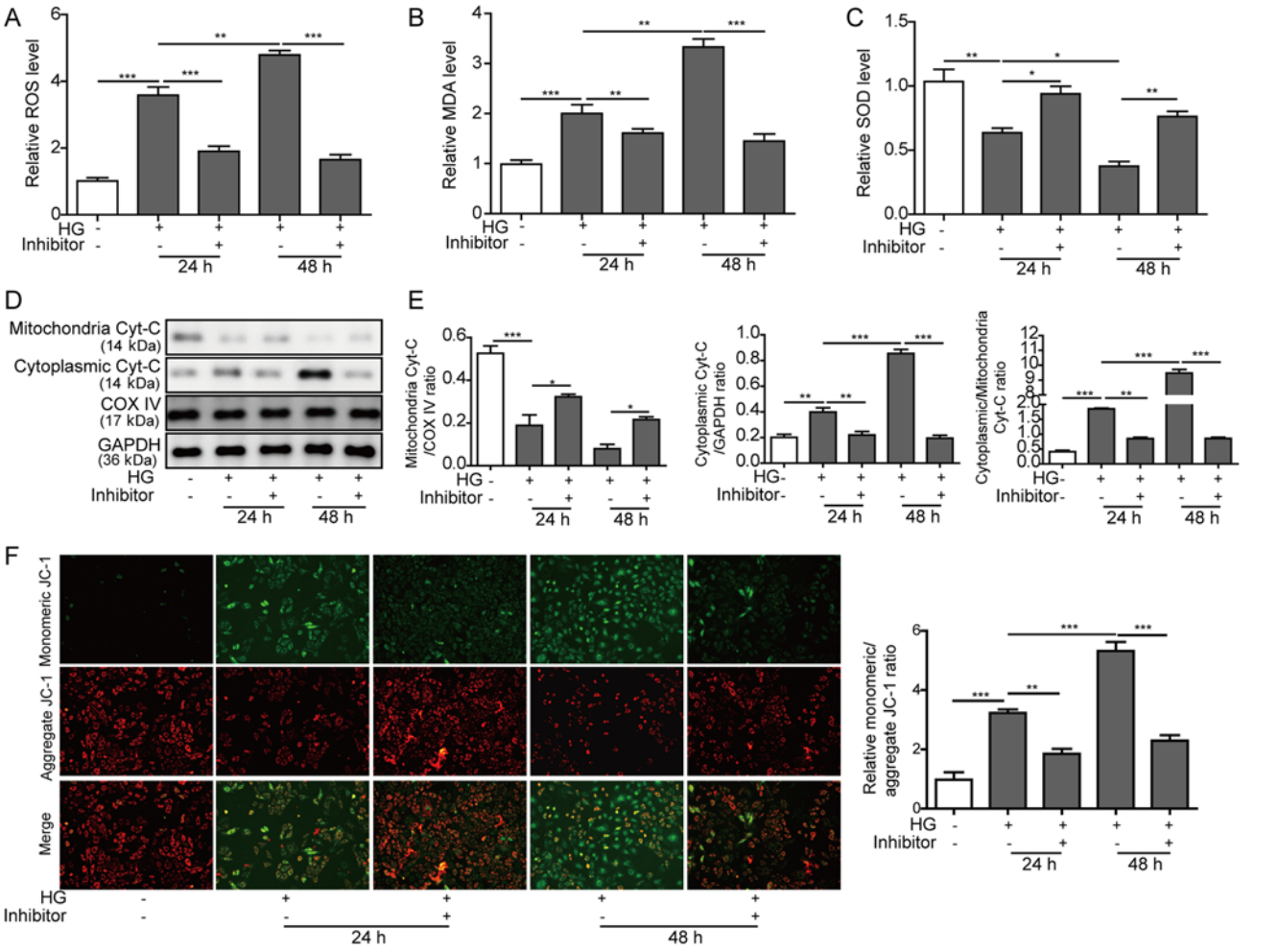

Figure 3. Effects of the miR-155 inhibitor on the oxidative stress and mitochondrial damage induced by HG. H9C2 cells were treated with HG and co-transfected with or without miR-155 inhibitor for 24 and 48 h. (A) Intracellular ROS levels were measured with the DCFH-DA assay. (B) MDA levels were measured with an MDA assay kit. (C) SOD levels were measured with a SOD assay kit. (D) Protein expression levels of mitochondrial and cytoplasmic Cyt-*c* were assessed by western blot analysis; COX IV and GAPDH were used as the loading controls for mitochondrial and cytoplasmic fractions, respectively. (E) Relative expression levels of mitochondrial and cytoplasmic Cyt-*c*, and the ratio of the normalized cytoplasmic/mitochondrial Cyt-*c* levels presented. (F) Mitochondrial membrane potential of was measured by JC-1 assay. The ratios of monomeric JC-1/aggregated JC-1 are presented on the right. Data are presented as the mean ± SD from three independent experiments. *P<0.05, **P<0.01 and ***P<0.001. COX IV, cytochrome-*c* oxidase subunit IV; Cyt-*c*, cytochrome-*c*; HG, high glucose; MDA, malonaldehyde; miR-155, microRNA 155; ROS, reactive oxygen species; SOD, Superoxide dismutase.

inhibition on cardiac fibrosis, western blot analyses was performed to assess the protein expression levels of collagen I and α-SMA in HG-treated H9C2 cells with or without miR-155 inhibitor transfection. It was demonstrated that HG treatment increased the protein expression levels of collagen I and α-SMA in a time-dependent manner, and miR-155 inhibition decreased these expression levels (Fig. 5A and B). The mRNA expression levels of collagen I and α-SMA after HG treatment and miR-155 inhibitor transfection were consistent with the protein expression levels described above (Fig. 5C). Collectively, the present results indicated that the miR-155 inhibitor may ameliorate cardiac fibrosis induced by HG.

Nrf2/HO-1 signaling is required to maintain the homeostasis of mitochondria in cardiomyocytes after HG treatment. To further examine the role of the Nrf2/HO-1 signaling pathway in the homeostasis of mitochondrial function, Nrf2 expression was knocked down using shRNA in HG-treated H9C2 cells transfected with the miR-155 inhibitor. To assess the transfection efficiency of shNrf2, western blotting was used to examine the protein expression level of Nrf2. It was shown that the protein expression level of Nrf2 was significantly decreased after shNrf2 transfection for 48 h (Fig. 6A). The protein expression levels of the Nrf2 and HO-1 were then examined in H9C2 cells at 48 h after transfection of miR-155 inhibitor and shNrf2. It was found that both Nrf2 and HO-1 protein expression levels were reduced in H9C2 cells after HG treatment, whereas miR-155 inhibition partially rescued their expression (Fig. 6B). However, Nrf2 knockdown significantly suppressed the protein expression levels of Nrf2 and HO-1 compared with the HG+miR-155 inhibitor+shNC group (Fig. 6B).

To assess the homeostasis of mitochondria, ROS, MDA and SOD levels were measured in HG-treated H9C2 cells at 48 h. It was shown that HG treatment significantly increases ROS and MDA expression levels and decreased SOD levels in H9C2 cells, whereas miR-155 inhibition reversed these phenotypes (Figs. 3A-C and 6C-E). Nrf2 knockdown reversed the effects of the miR-155 inhibitor, leading to elevated

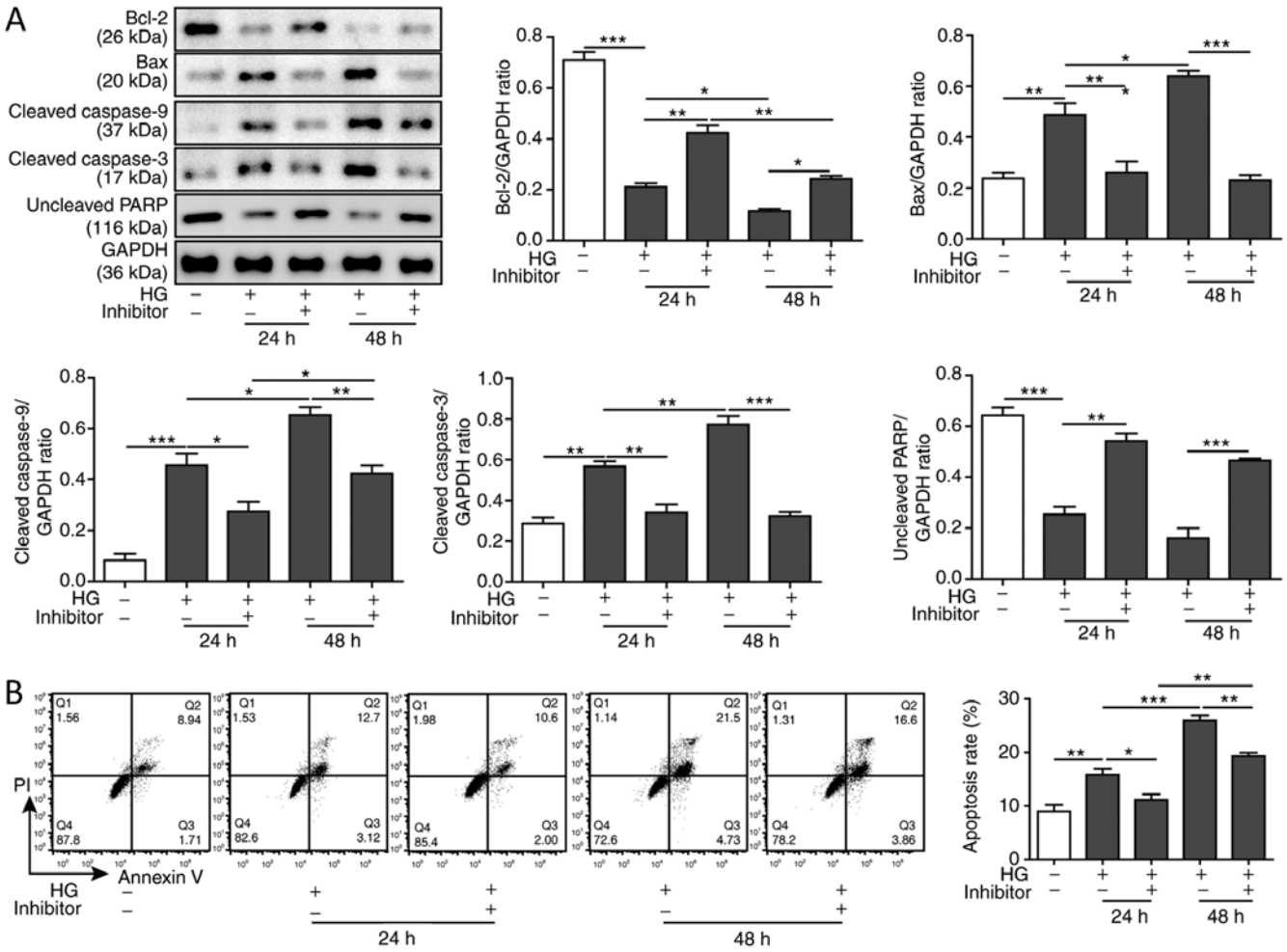

Figure 4. Effect of the miR-155 inhibitor on apoptosis induced by HG. H9C2 cells were treated with HG and co-transfected with or without miR-155 inhibitor for 24 and 48 h. (A) Expression levels of the apoptosis-related proteins were assessed by western blot analysis and semi-quantitated; GAPDH was used as the loading control and for normalization. (B) Apoptotic rates were determined by Annexin V-FITC/PI staining and flow cytometry. Data are presented as the mean ± SD from three independent experiments. *P<0.05, **P<0.01 and ***P<0.001. miR-155, microRNA 155; HG, high glucose; PARP, poly (ADP-ribose) polymerase; PI, propidium iodide.

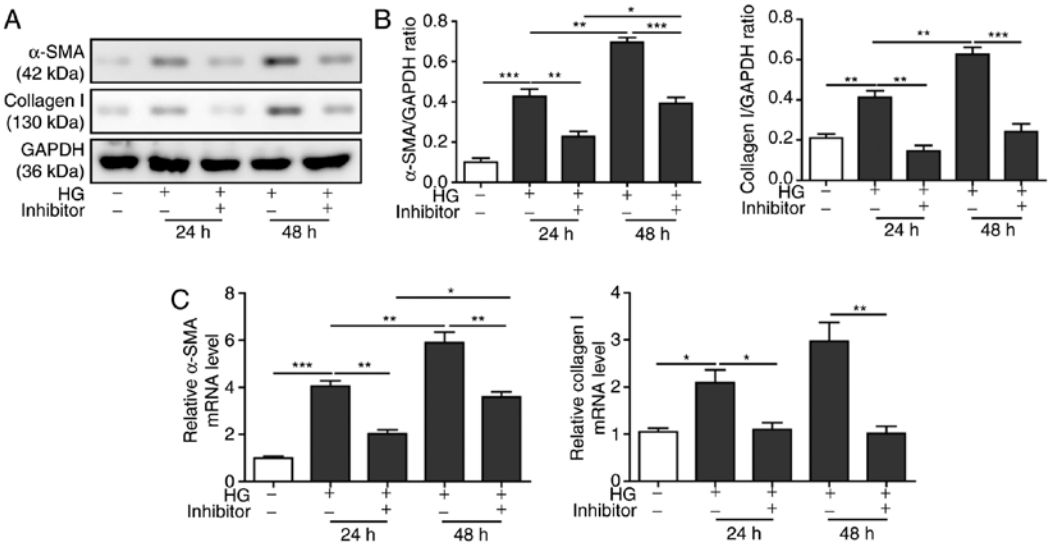

Figure 5. Effect of the miR-155 inhibitor on the cardiac fibrosis induced by HG. H9C2 cells were treated with HG and co-transfected with or without miR-155 inhibitor for 24 and 48 h. (A) Protein expression levels of α-SMA and collagen I were analyzed by western blotting; GAPDH was used as the loading control. (B) Semi-quantification of western blotting results of α-SMA and collagen I expression levels after normalization to the level of GAPDH. (C) Relative mRNA expression levels of α-SMA and collagen I were measured by reverse transcription-quantitative PCR. Data are presented as the mean ± SD from three independent experiments. *P<0.05, **P<0.01 and ***P<0.001. α-SMA, α-smooth muscle actin; HG, high glucose; miR-155, microRNA 155.

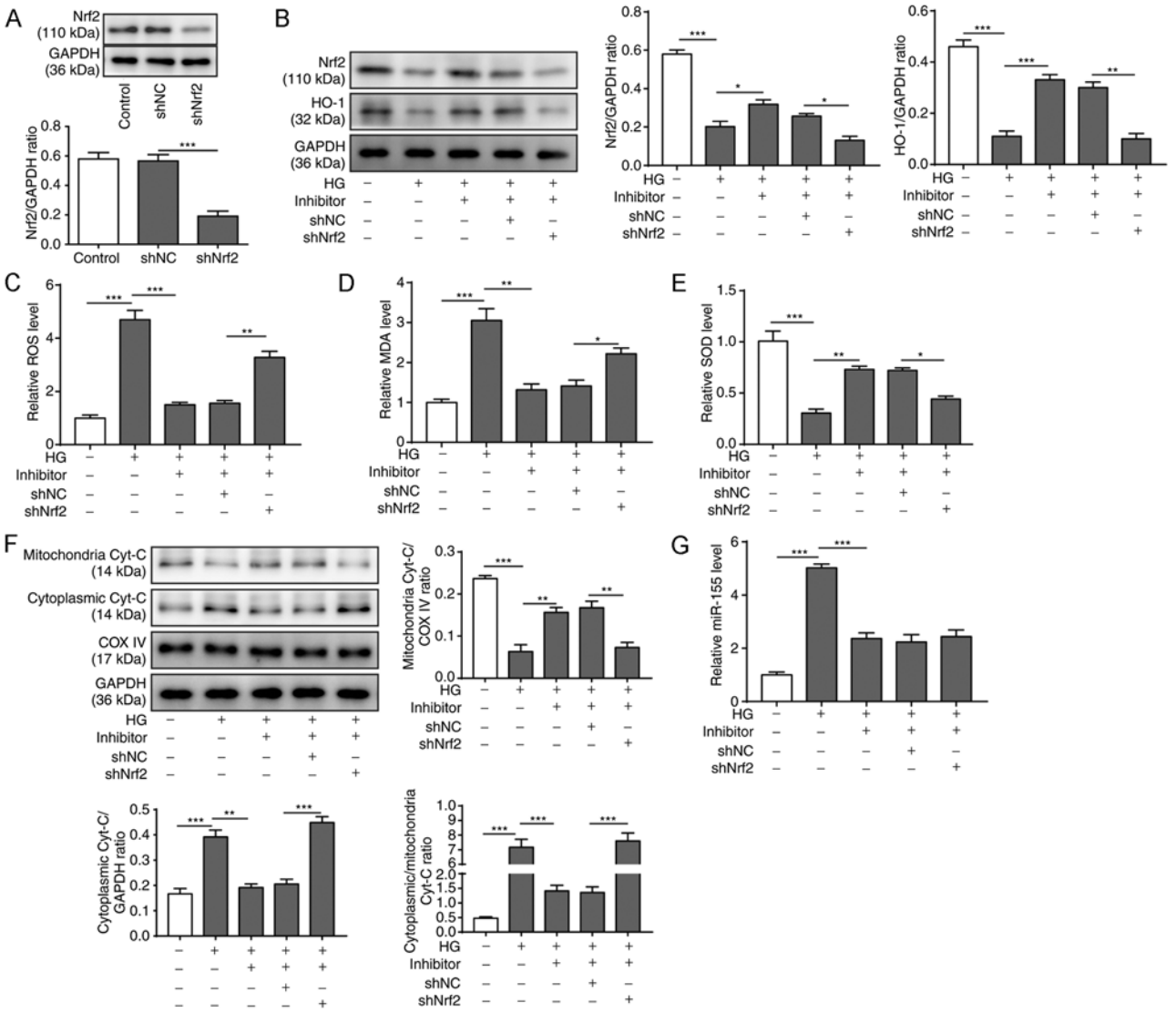

Figure 6. Nrf2/HO-1 signaling is required to maintain the homeostasis of mitochondria in cardiomyocytes after HG treatment. HG-treated H9C2 cells were co-transfected with or without miR-155 inhibitor and with or without sh-Nrf2 for 48 h. (A) Transfection efficiency of shNC and shNrf2 in H9C2 cells was assessed by western blot analyses. (B) Protein expression levels of Nrf2 and HO-1 in H9C2 cells were measured by western blot analyses; GAPDH was used as the loading control. Intracellular (C) ROS, (D) MDA and (E) SOD expression levels were measured with a DCFH-DA assay kit, an MDA assay kit and a SOD assay kit, respectively. (F) Protein expression levels of mitochondrial and cytoplasmic Cyt-*c* were assessed by western blot analyses; COX IV and GAPDH were used as the loading controls for the mitochondrial and cytoplasmic fractions, respectively. (G) Relative mRNA expression levels of miR-155 were measured by reverse transcription-quantitative PCR. Data are presented as the mean ± SD from three independent experiments. *P<0.05, **P<0.01 and ***P<0.001. COX IV, cytochrome *c* oxidase subunit IV; Cyt-*c*, cytochrome-*c*; DCFH-DA, dichloro-dihydro-fluorescein diacetate; HG, high glucose; HO-1, heme oxygenase-1; MDA, malonaldehyde; miR-155, microRNA 155; NC, negative control; Nrf2, nuclear factor erythroid-2-related factor 2; sh, short hairpin RNA; ROS, reactive oxygen species; SOD, superoxide dismutase.

ROS and MDA expression levels, and reduced SOD levels (Fig. 6C-E), which suggested that Nrf2 may be required for mitochondrial homeostasis.

Moreover, western blotting was used to investigate the mitochondrial and cytoplasmic expression levels of Cyt-*c* in H9C2 cells after the treatment (Fig. 6F). The results revealed that mitochondrial Cyt-*c* was reduced by HG treatment, increased by miR-155 inhibition, and subsequently reduced by Nrf2 knockdown, whereas the cytoplasmic Cyt-*c* expression levels were opposite (Fig. 6F). The changes in mitochondrial and cytoplasmic Cyt-*c* expression following Nrf2 knockdown further demonstrated that Nrf2 may be essential for maintaining the normal function of mitochondria under HG conditions. Furthermore, RT-qPCR results demonstrated that the miR-155 inhibitor suppressed the expression of miR-155 in the H9C2 cells after HG treatment, and subsequent Nrf2 knockdown had no significant effect on miR-155 expression level (Fig. 6G). Taken together, these results demonstrated that the Nrf2/HO-1 signaling pathway may be required for the homeostasis of the mitochondria in cardiomyocytes after HG treatment.

Nrf2/HO-1 signaling is essential for the effects of the miR-155 inhibitor on the apoptosis and cardiac fibrosis induced by HG. To investigate whether the Nrf2/HO-1 signaling pathway is required for miR-155 inhibitor-induced suppression of apoptosis and/or fibrosis of cardiomyocytes, Nrf2 was knocked down by shRNA in H9C2 cells transfected with

miR-155 inhibitor and treated with HG for 48 h. The western blotting results demonstrated that the expression level of the anti-apoptotic protein Bcl-2 was reduced by HG treatment, increased by miR-155 inhibition and decreased after Nrf2 knockdown (Fig. 7A). By contrast, the expression levels of the pro-apoptotic protein Bax were increased by HG treatment, reduced by miR-155 inhibition and increased following Nrf2 knockdown. Cleaved caspase-3 and cleaved caspase-9 protein expression levels were increased in H9C2 cells after Nrf2 knockdown, whereas uncleaved PARP expression levels were decreased (Fig. 7A). miR-155 inhibition significantly decreased the apoptotic rate of H9C2 cells after HG treatment, whereas Nrf2 knockdown enhanced the apoptosis of H9C2 cells (Fig. 7B).

To evaluate the effect of Nrf2 knockdown on the extent of miR-155-induced fibrosis of the cardiomyocytes, the expression levels of a-SMA and collagen I were measured by western blotting and RT-qPCR (Fig. 7C and D, respectively). The results showed that both a-SMA and collagen I were upregulated in HG-treated H9C2 cells and were downregulated after miR-155 inhibition; however, Nrf2 knockdown led to increased expression of a-SMA and collagen I at both the protein and mRNA level. Collectively, these results indicated that the Nrf2/HO-1 signaling pathway may be the underlying mechanism for miR-155 inhibitor-induced inhibition of apoptosis and fibrosis of the cardiomyocytes in response to HG treatment.

Discussion

Progressive cardiac fibrosis is associated with myocardial infarction, hypertrophy, hypertension, heart failure and other cardiovascular diseases (1). However, current therapies for cardiac fibrosis are severely limited and inefficient (32). To develop strategies against cardiac fibrosis, the pathogenesis and the complex regulatory network of these pathologies must be investigated in greater depth. To the best of our knowledge, the present study is the first to report the role of miR-155 in regulating oxidative stress, mitochondrial injury and myocardial apoptosis via the Nrf2/HO-1 signaling pathway in cardiac fibrosis, using HG-induced H9C2 rat cardiomyocytes as an *in vitro* model.

A previous clinical study has shown that myocardial damage associated with diabetic cardiomyopathy is related to glucose level (33). In addition, dysregulation of miRNAs is associated with cardiac fibrosis (34). To investigate whether miR-155 affected oxidative stress, mitochondrial damage, apoptosis, as well as extracellular matrix accumulation, the present study aimed to determine the underlying mechanisms of these processes in cardiomyocytes under HG conditions. It was demonstrated that expression levels of collagen I and α-SMA were significantly upregulated after HG treatment. In addition, miR-155 expression level was increased in cardiomyocytes by induced glucotoxicity; a finding that was consistent with previous studies on miR-155 expression in human renal glomerular endothelial cells and endothelial progenitor cells in HG microenvironments (35,36). Moreover, the present results indicated that inhibiting miR-155 suppressed glucotoxicity-induced apoptosis of cardiomyocytes, whereas overexpression of miR-155 increased the number of apoptotic cells. Similar phenotypes have also been reported in HG-treated endothelial progenitor cells and acute myeloid leukemia cells (36,37). The present study demonstrated that miR-155 may be implicated in HG-induced cardiac fibrosis and is positively associated with apoptosis.

The present results showed that the Nrf2/HO-1 signaling pathway was impaired under HG conditions in a time-dependent manner, as indicated by decreased endonuclear Nrf2 and HO-1 expression levels but increased cytoplasmic Nrf2 expression; this has also been reported in previous studies (38-41). However, another previous study found that Nrf2 expression and nuclear translocation are enhanced after HG exposure (42). These contradicting conclusions indicated that the details of Nrf2 functions in cardiomyocytes are complex. Excessive Nrf2 protein can be ubiquitinated and degraded through the ubiquitin-proteasome system, which is regulated by the miR-29/Kelch Like ECH Associated Protein 1 axis (43). We hypothesized that, over a short time period, such as <24 h after the initial HG challenge, cardiomyocytes show increased Nrf2 expression levels to counteract the induced oxidative stress and protect themselves from oxidant-induced damage; however, over a longer period of oxidative stress, such as 48 h, Nrf2 is ubiquitinated and degraded. Therefore, a precise tuning mechanism likely maintains the homeostasis of Nrf2 and protects cardiomyocytes from oxidative stress-induced apoptosis. HG-induced impairment of the Nrf2/HO-1 pathway is implicated in the disruption of homeostasis by oxidative stress in cardiomyocytes. However, the complex regulatory network behind cardiac fibrosis also comprises other pathways, such as the TGFb1/SMAD2 signaling pathway, as reported in a diabetes-induced cardiac fibrosis in mice (11). The present results suggested that the miR-155 inhibitor partially rescued the impaired Nrf2/HO-1 signaling pathway induced by HG, which was reflected by the significant increase in nuclear translocation of Nrf2 and the upregulated expression level of HO-1. Therefore, miR-155 may play a pivotal role in the regulation of the Nrf2/HO-1 signaling pathway. Previous studies have demonstrated that miR-155 directly targets Nrf2 in septic liver injury and diabetic peripheral neuropathy (44,45). However, the precise mechanism of miR-155 in the regulation of the Nrf2/HO-1 pathway in cardiac fibrosis requires further investigation.

Previous studies have shown that the Nrf2/HO-1 pathway is extensively involved in the regulation of oxidative stress (46), mitochondrial injury (47) and apoptosis (48), and these phenotypes contribute to the pathogenesis of cardiac fibrosis (46,49). Thus, the present study focused on oxidative stress, mitochondrial injury and apoptosis in subsequent experiments. In the present study, H9C2 cells treated with HG showed enhanced accumulation of ROS and MDA, and lower expression levels of SOD, which indicated that after HG treatment cardiomyocytes were under substantial oxidative stress. Previous studies have also revealed that HG induces oxidative stress and apoptosis in cardiac microvascular endothelial cells (50) and in human umbilical vein endothelial cells (51). In addition, the increased ratio of cytoplasmic Cyt-*c* to mitochondrial Cyt-*c* indicated the presence of mitochondrial injury upon HG induction, which coincides with a previous study showing that HG and high-fat conditions lead to mitochondrial dysfunction and apoptosis in cardiomyocytes (52). Directly measuring the

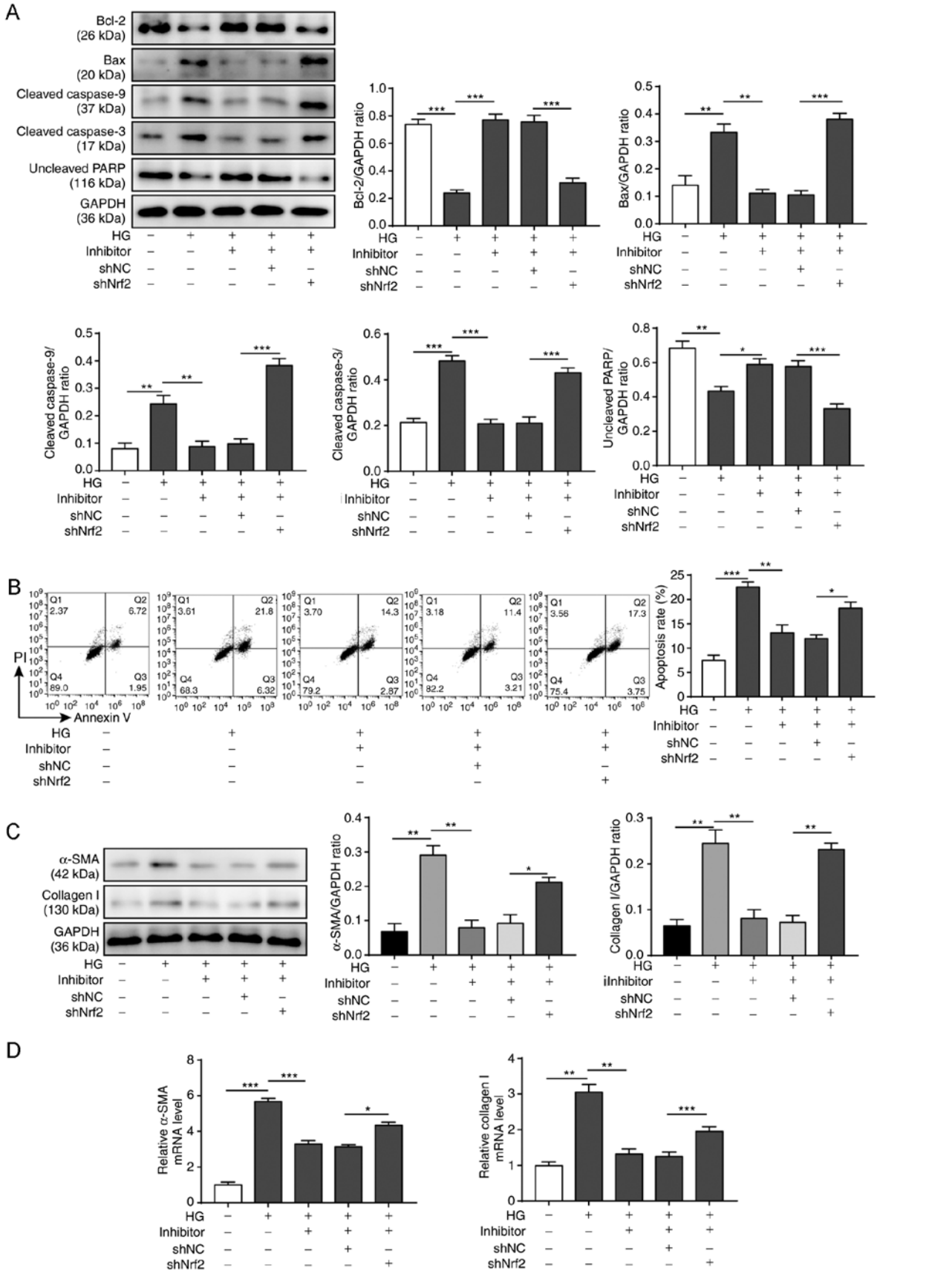

Figure 7. Effects of miR-155 inhibitor on Nrf2/HO-1 signaling and HG-induced apoptosis and cardiac fibrosis. HG-treated H9C2 cells were co-transfected with or without miR-155 inhibitor and with or without sh-Nrf2 for 48 h. (A) Expression levels of apoptosis-related proteins were assessed by western blot analyses; GAPDH was used as the loading control. (B) Apoptotic rates of H9C2 cells were examined by Annexin V-FITC/PI staining and flow cytometry. (C) Protein expression levels of α-SMA and collagen I were analyzed by western blotting; GAPDH was used as the loading control. (D) Relative mRNA expression levels of a-SMA and collagen I RNA were measured by reverse transcription-quantitative PCR. Data are presented as the mean ± SD from three independent experiments. *P<0.05, **P<0.01 and ***P<0.001. α-SMA, α-smooth muscle actin; HG, high glucose; HO-1, heme oxygenase-1; miR-155, microRNA 155; NC, negative control; Nrf2, nuclear factor erythroid-2-related factor 2; sh, short hairpin RNA; PARP, poly (ADP-ribose) polymerase; PI, propidium iodide.

mitochondrial ROS level could reveal the oxidative stress accumulation in mitochondria upon HG treatment; however, this measurement was not performed in the present study due to the facility limitations. Moreover, the dissipation of mitochondrial membrane potential in the H9C2 cells further supported the hypothesis that mitochondrial function was impaired upon HG treatment, and this phenomenon has also been reported in previous studies with respect to 3T3-L1 adipocytes and human peritoneal mesothelial cells (53,54). Elevated levels of oxidative stress and mitochondrial injury resulted in increased numbers of apoptotic cells, as indicated in the present study by increased expression levels of pro-apoptotic proteins and reduced expression levels of anti-apoptotic proteins. The results also demonstrated that apoptosis induced by HG is caspase-9-dependent, which is consistent with previous studies investigating human endothelial cells and periodontal ligament fibroblasts under HG conditions (55,56). Moreover, miR-155 inhibition significantly suppressed oxidative stress, mitochondrial injury and apoptosis. Therefore, miR-155 may exert its pro-fibrosis function by impairing the Nrf2/HO-1 signaling pathway to cause oxidative stress, mitochondrial injury and myocardial apoptosis. Moreover, the importance of Nrf2/HO-1 signaling in the homeostasis of mitochondria upon HG treatment was indicated in subsequent experiments, in which Nrf2 was knocked down. However, further investigation is required to obtain more details on this mechanism.

The present study also investigated the function of miR-155 attenuation on cardiac fibrosis. High expression levels of α-SMA and collagen I were significantly decreased after the miR-155 inhibition. Wei *et al* (9) found that miR-155 deficiency ameliorated the progression of angiotensin II-induced cardiac fibrosis in mice. During the wound healing process, acute reduction in miR-155 expression resulted in a milder fibrosis phenotype, which was acquired by a suppressed inflammatory response, and also accelerated the healing rate (57). Therefore, targeting miR-155 may ameliorate cardiac fibrosis caused by HG. In addition, the present study found that miR-155 may exert its effect partially via Nrf2/HO-1 signaling, as indicated by the results from Nrf2 knockdown experiments, which showed that Nrf2 knockdown compromised the effects of miR-155 inhibition on oxidative stress and cell apoptosis, as well as a-SMA and collagen I accumulation in HG-treated H9C2 cells.

In conclusion, miR-155 may regulate the pathogenesis of cardiac fibrosis via the Nrf2/HO-1 signaling pathway. The present study results not only elucidated a novel pathway for the pathogenesis of cardiac fibrosis induced by HG, but also identified the potential of miR-155 as a therapeutic for cardiac fibrosis. However, this conclusion is based mainly on *in vitro* cellular assays, thus *in viv*o experiments are required to further investigate these effects. Therefore, generating specific transgenic mice and evaluating the clinical relevance of miR-155 using human samples are required in follow-up studies.

Acknowledgements

Not applicable.

Funding

No funding was received.

Availability of data and materials

The datasets used and/or analyzed during the current study are available from the corresponding author on reasonable request.

Authors' contributions

YL conceptualized and designed the study, drafted and revised the manuscript, acquired funding and supervised the research group. CQW analyzed the data. JZD, YL and QH performed the experiments and analyzed the data. YL and CQW edited the manuscript. All authors read and approved the final manuscript.

Ethics approval and consent to participate

Not applicable.

Patient consent for publication

Not applicable.

Competing interests

The authors declare that they have no competing interests.

References

1. Worke LJ, Barthold JE, Seelbinder B, Novak T, Main RP, Harbin SL and Neu CP: Densification of type I collagen matrices as a model for cardiac fibrosis. Adv Healthc Mater 6: 1700114, 2017.
2. Murtha LA, Schuliga MJ, Mabotuwana NS, Hardy SA, Waters DW, Burgess JK, Knight DA and Boyle AJ: The processes and mechanisms of cardiac and pulmonary fibrosis. Front Physiol 8: 777, 2017.
3. Louridas GE and Lourida KG: Systems biology and biomechanical model of heart failure. Curr Cardiol Rev 8: 220-230, 2012.
4. Zhang WW, Bai F, Wang J, Zheng RH, Yang LW, James EA and Zhao ZQ: Edaravone inhibits pressure overload-induced cardiac fibrosis and dysfunction by reducing expression of angiotensin II AT1 receptor. Drug Des Devel Ther 11: 3019-3033, 2017.
5. Michael LH, Taffet GE, Entman ML, Reddy AK, Hartley CJ and Frangogiannis NG: Chapter 2.6-The Cardiovascular System. In: The Laboratory Mouse (Second Edition). Hedrich HJ (ed) Academic Press, Boston, pp 241-270, 2012.
6. Asbun J and Villarreal FJ: The pathogenesis of myocardial fibrosis in the setting of diabetic cardiomyopathy. J Am Coll Cardiol 47: 693-700, 2006.
7. Bharati S and Lev M: Cardiac conduction system involvement in sudden death of obese young people. Am Heart J 129: 273-281, 1995.
8. Dei Cas A, Khan SS, Butler J, Mentz RJ, Bonow RO, Avogaro A, Tschoepe D, Doehner W, Greene SJ, Senni M, *et al*: Impact of diabetes on epidemiology, treatment, and outcomes of patients with heart failure. JACC Heart Fail 3: 136-145, 2015.
9. Wei Y, Yan X, Yan L, Hu F, Ma W, Wang Y, Lu S, Zeng Q and Wang Z: Inhibition of microRNA-155 ameliorates cardiac fibrosis in the process of angiotensin II-induced cardiac remodeling. Mol Med Rep 16: 7287-7296, 2017.
10. Quiat D and Olson EN: MicroRNAs in cardiovascular disease: From pathogenesis to prevention and treatment. J Clin Invest 123: 11-18, 2013.
11. Zhang D, Cui Y, Li B, Luo X, Li B and Tang Y: miR-155 regulates high glucose-induced cardiac fibrosis via the TGF-β signaling pathway. Mol Biosyst 13: 215-224, 2016.
12. Seok HY, Chen J, Kataoka M, Huang ZP, Ding J, Yan J, Hu X and Wang DZ: Loss of MicroRNA-155 protects the heart from pathological cardiac hypertrophy. Circ Res 114: 1585-1595, 2014.

13. Tran PL, Tran PT, Tran HNK, Lee S, Kim O, Min BS and Lee JH: A prenylated flavonoid, 10-oxomornigrol F, exhibits anti-inflammatory effects by activating the Nrf2/heme oxygenase-1 pathway in macrophage cells. Int Immunopharmacol 55: 165-173, 2018.
14. Chen RR, Fan XH, Chen G, Zeng GW, Xue YG, Liu XT and Wang C: Irisin attenuates angiotensin II-induced cardiac fibrosis via Nrf2 mediated inhibition of ROS/ TGFβ1/Smad2/3 signaling axis. Chem Biol Interact 302: 11-21, 2019.
15. Meng Z, Li HY, Si CY, Liu YZ and Teng S: Asiatic acid inhibits cardiac fibrosis throughNrf2/HO-1 and TGF-β1/Smads signaling pathways in spontaneous hypertension rats. Int Immunopharmacol 74: 105712, 2019.
16. Jeong JY, Cha HJ, Choi EO, Kim CH, Kim GY, Yoo YH, Hwang HJ, Park HT, Yoon HM and Choi YH: Activation of the Nrf2/HO-1 signaling pathway contributes to the protective effects of baicalein against oxidative stress-induced DNA damage and apoptosis in HEI193 Schwann cells. Int J Med Sci 16: 145-155, 2019.
17. Abraham NG and Kappas A: Heme oxygenase and the cardiovascular-renal system. Free Radic Biol Med 39: 1-25, 2005.
18. Chen M, Samuel VP, Wu Y, Dang M, Lin Y, Sriramaneni R, Sah SK, Chinnaboina GK and Zhang G: Nrf2/HO-1 mediated protective activity of genistein against doxorubicin-induced cardiac toxicity. J Environ Pathol Toxicol Oncol 38: 143-152, 2019.
19. Chen C, Jiang X, Gu S and Zhang Z: MicroRNA-155 regulates arsenite-induced malignant transformation by targeting Nrf2-mediated oxidative damage in human bronchial epithelial cells. Toxicol Lett 278: 38-47, 2017.
20. Wan C, Han R, Liu L, Zhang F, Li F, Xiang M and Ding W: Role of miR-155 in fluorooctane sulfonate-induced oxidative hepatic damage via the Nrf2-dependent pathway. Toxicol Appl Pharmacol 295: 85-93, 2016.
21. Gu S, Lai Y, Chen H, Liu Y and Zhang Z: miR-155 mediates arsenic trioxide resistance by activating Nrf2 and suppressing apoptosis in lung cancer cells. Sci Rep 7: 12155, 2017.
22. Hu M, Ye P, Liao H, Chen M and Yang F: Metformin protects H9C2 cardiomyocytes from high-glucose and hypoxia/reoxygenation injury via inhibition of reactive oxygen species generation and inflammatory responses: Role of AMPK and JNK. J Diabetes Res 2016: 2961954, 2016.
23. Bugyei-Twum A, Advani A, Advani SL, Zhang Y, Thai K, Kelly DJ and Connelly KA: High glucose induces Smad activation via the transcriptional coregulator p300 and contributes to cardiac fibrosis and hypertrophy. Cardiovasc Diabetol 13: 89, 2014.
24. Livak KJ and Schmittgen TD: Analysis of relative gene expression data using real-time quantitative PCR and the 2(-Delta Delta C(T)) method. Methods 25: 402-408, 2001.
25. Ahmad A and Abdel Moneim AE: Indigofera oblongifolia prevents lead acetate-induced hepatotoxicity, oxidative stress, fibrosis and apoptosis in rats. PLoS One 11: e0158965, 2016.
26. Hüttemann M, Pecina P, Rainbolt M, Sanderson TH, Kagan VE, Samavati L, Doan JW and Lee I: The multiple functions of cytochrome c and their regulation in life and death decisions of the mammalian cell: From respiration to apoptosis. Mitochondrion 11: 369-381, 2011.
27. Garrido C, Galluzzi L, Brunet M, Puig PE, Didelot C and Kroemer G: Mechanisms of cytochrome c release from mitochondria. Cell Death Differ 13: 1423-1433, 2006.
28. Tsutsui H, Kinugawa S and Matsushima S: Mitochondrial oxidative stress and dysfunction in myocardial remodelling. Cardiovasc Res 81: 449-456, 2008.
29. Opferman JT and Kothari A: Anti-apoptotic BCL-2 family members in development. Cell Death Differ 25: 37-45, 2018.
30. Czabotar PE, Lessene G, Strasser A and Adams JM: Control of apoptosis by the BCL-2 protein family: Implications for physiology and therapy. Nat Rev Mol Cell Biol 15: 49-63, 2014.
31. Ma ZG, Yuan YP, Wu HM, Zhang X and Tang QZ: Cardiac fibrosis: New insights into the pathogenesis. Int J Biol Sci 14: 1645-1657, 2018.
32. Fang L, Murphy AJ and Dart AM: A Clinical perspective of anti-fibrotic therapies for cardiovascular disease. Front Pharmacol 8: 186-186, 2017.
33. Brahma MK, Pepin ME and Wende AR: My sweetheart is broken: Role of glucose in diabetic cardiomyopathy. Diabetes Metab J 41: 1-9, 2017.
34. Costantino S, Paneni F, Lüscher TF and Cosentino F: MicroRNA profiling unveils hyperglycaemic memory in the diabetic heart. Eur Heart J 37: 572-576, 2016.
35. Huang Y, Liu Y, Li L, Su B, Yang L, Fan W, Yin Q, Chen L, Cui T, Zhang J, *et al*: Involvement of inflammation-related miR-155 and miR-146a in diabetic nephropathy: implications for glomerular endothelial injury. BMC Nephrol 15: 142, 2014.
36. Gao J, Zhao G, Li W, Zhang J, Che Y, Song M, Gao S, Zeng B and Wang Y: miR-155 targets PTCH1 to mediate endothelial progenitor cell dysfunction caused by high glucose. Exp Cell Res 366: 55-62, 2018.
37. Palma CA, Al Sheikha D, Lim TK, Bryant A, Vu TT, Jayaswal V and Ma DD: MicroRNA-155 as an inducer of apoptosis and cell differentiation in Acute Myeloid Leukaemia. Mol Cancer 13: 79, 2014.
38. Song Y, Wen L, Sun J, Bai W, Jiao R, Hu Y, Peng X, He Y and Ou S: Cytoprotective mechanism of ferulic acid against high glucose-induced oxidative stress in cardiomyocytes and hepatocytes. Food Nutr Res 60: 30323, 2016.
39. You S, Qian J, Sun C, Zhang H, Ye S, Chen T, Xu Z, Wang J, Huang W and Liang G: An Aza resveratrol-chalcone derivative 6b protects mice against diabetic cardiomyopathy by alleviating inflammation and oxidative stress. J Cell Mol Med 22: 1931-1943, 2018.
40. Ying Y, Jin J, Ye L, Sun P, Wang H and Wang X: Phloretin prevents diabetic cardiomyopathy by dissociating Keap1/Nrf2 complex and inhibiting oxidative stress. Front Endocrinol (Lausanne) 9: 774, 2018.
41. Li L, Luo W, Qian Y, Zhu W, Qian J, Li J, Jin Y, Xu X and Liang G: Luteolin protects against diabetic cardiomyopathy by inhibiting NF-κB-mediated inflammation and activating the Nrf2-mediated antioxidant responses. Phytomedicine 59: 152774, 2019.
42. Tsai CY, Wen SY, Cheng SY, Wang CH, Yang YC, Viswanadha VP, Huang CY and Kuo WW: Nrf2 activation as a protective feedback to limit cell death in high glucose-exposed cardiomyocytes. J Cell Biochem 118: 1659-1669, 2017.
43. Zhou L, Xu DY, Sha WG, Shen L, Lu GY, Yin X and Wang MJ: High glucose induces renal tubular epithelial injury via Sirt1/NF-kappaB/microR-29/Keap1 signal pathway. J Transl Med 13: 352, 2015.
44. Yang ZB, Chen WW, Chen HP, Cai SX, Lin JD and Qiu LZ: MiR-155 aggravated septic liver injury by oxidative stress-mediated ER stress and mitochondrial dysfunction via targeting Nrf-2. Exp Mol Pathol 105: 387-394, 2018.
45. Chen J, Li C, Liu W, Yan B, Hu X and Yang F: miRNA-155 silencing reduces sciatic nerve injury in diabetic peripheral neuropathy. J Mol Endocrinol 63: 227-238, 2019.
46. Kosuru R, Kandula V, Rai U, Prakash S, Xia Z and Singh S: Pterostilbene decreases cardiac oxidative stress and inflammation via activation of AMPK/Nrf2/HO-1 pathway in fructose-fed diabetic rats. Cardiovasc Drugs Ther 32: 147-163, 2018.
47. Holmström KM, Kostov RV and Dinkova-Kostova AT: The multifaceted role of Nrf2 in mitochondrial function. Curr Opin Toxicol 1: 80-91, 2016.
48. Liang J, Li L, Sun Y, He W, Wang X and Su Q: The protective effect of activating Nrf2/HO-1 signaling pathway on cardiomyocyte apoptosis after coronary microembolization in rats. BMC Cardiovasc Disord 17: 272, 2017.
49. Zhang YF, Meng NN, Li HZ, Wen YJ, Liu JT, Zhang CL, Yuan XH and Jin XD: Effect of naringin on oxidative stress and endoplasmic reticulum stress in diabetic cardiomyopathy. Zhongguo Zhong Yao Za Zhi 43: 596-602, 2018 (In Chinese).
50. Peng C, Ma J, Gao X, Tian P, Li W and Zhang L: High glucose induced oxidative stress and apoptosis in cardiac microvascular endothelial cells are regulated by FoxO3a. PLoS One 8: e79739, 2013.
51. Wang R, Lu L, Guo Y, Lin F, Chen H, Chen W and Chen M: Effect of glucagon-like peptide-1 on high-glucose-induced oxidative stress and cell apoptosis in human endothelial cells and its underlying mechanism. J Cardiovasc Pharmacol 66: 135-140, 2015.
52. Zhang M, Niu X, Hu J, Yuan Y, Sun S, Wang J, Yu W, Wang C, Sun D and Wang H: Lin28a Protects against hypoxia/reoxygenation induced cardiomyocytes apoptosis by alleviating mitochondrial dysfunction under high glucose/high fat conditions. PLoS One 9: e110580, 2014.
53. Gao CL, Zhu C, Zhao YP, Chen XH, Ji CB, Zhang CM, Zhu JG, Xia ZK, Tong ML and Guo XR: Mitochondrial dysfunction is induced by high levels of glucose and free fatty acids in 3T3-L1 adipocytes. Mol Cell Endocrinol 320: 25-33, 2010.

54. Hung KY, Liu SY, Yang TC, Liao TL and Kao SH: High-dialysate-glucose-induced oxidative stress and mitochondrial-mediated apoptosis in human peritoneal mesothelial cells. Oxid Med Cell Longev 2014: 642793-642793, 2014.
55. Ho FM, Liu SH, Liau CS, Huang PJ and Lin-Shiau SY: High glucose-induced apoptosis in human endothelial cells is mediated by sequential activations of c-Jun NH(2)-terminal kinase and caspase-3. Circulation 101: 2618-2624, 2000.
56. Liu J, Wu Y, Wang B, Yuan X and Fang B: High levels of glucose induced the caspase-3/PARP signaling pathway, leading to apoptosis in human periodontal ligament Fibroblasts. Cell Biochem Biophys 66: 229-237, 2013.
57. Yang LL, Liu JQ, Bai XZ, Fan L, Han F, Jia WB, Su LL, Shi JH, Tang CW and Hu DH: Acute downregulation of miR-155 at wound sites leads to a reduced fibrosis through attenuating inflammatory response. Biochem Biophys Res Commun 453: 153-159, 2014.